Scilight

Durability and Sustainability

https://www.sciltp.com/journals/ds

Article

Comparative Investigation on Performance of Fly Ash-Based Geopolymer Paste Subjected to Na_2SO_4 and $MgSO_4$ Solution

Xiaoshuang Shi [1], Tao Long [1], Hongen Zhang [2] and Qingyuan Wang [1,3,*]

[1] Failure Mechanics & Engineering Disaster Prevention and Mitigation Key Laboratory of Sichuan Province, College of Architecture and Environment, Sichuan University, Chengdu 610065, China
[2] Key Laboratory of Advanced Civil Engineering Materials of Ministry of Education, School of Materials Science and Engineering, Tongji University, Shanghai 201804, China
[3] State Key Laboratory of Hydraulics and Mountain River Engineering, Sichuan University, Chengdu 610065, China
* Correspondence: wangqy@scu.edu.cn

How To Cite: Shi, X.; Long, T.; Zhang, H.; et al. Comparative Investigation on Performance of Fly Ash-Based Geopolymer Paste Subjected to Na_2SO_4 and $MgSO_4$ Solution. *Durability and Sustainability* **2026**, *1*(1), 2.

Received: 9 April 2026
Revised: 19 August 2026
Accepted: 31 August 2026
Published: 14 September 2026

Abstract: The present study aimed to evaluate the comparative deterioration mechanism of sulfate solution on the fly ash based geopolymer paste (GP) by soaking in 8% Na_2SO_4 and 8% $MgSO_4$ solutions up to 120 days. X-ray CT, SEM, EDS, XRD, FTIR and TGA/DTG were used to characterize the changes in microstructure and products under sulfate attack. Furthermore, the corrosion solution was also analyzed by ICP-OES and pH analysis. The results showed that Na_2SO_4 and $MgSO_4$ induced distinctly different deterioration behaviors. After 120 days of immersion, the compressive strength loss rates reached 40.2% and 34.0% in Na_2SO_4 and $MgSO_4$ solutions, respectively. Na_2SO_4 exposure mainly caused surface exfoliation and significant alteration of the sodium aluminosilicate hydrate (N-A-S-H) gel structure, accompanied by the formation of analcime-containing phases and salt crystallization. In contrast, $MgSO_4$ exposure promoted the transformation of N-A-S-H gel into magnesium aluminosilicate hydrate (M-A-S-H) gel and induced crystallization-related crack development. Although $MgSO_4$ attack generated more visible cracking, Na_2SO_4 resulted in greater strength deterioration. These findings indicate that the deterioration of GP in Na_2SO_4 solution is governed primarily by gel alteration and exfoliation, whereas $MgSO_4$ attack involves both gel transformation and crystallization-induced cracking. The study provides new insights into the sulfate attack mechanisms of fly ash-based geopolymers and supports their durability assessment in sulfate-rich environments.

Keywords: fly ash-based geopolymer paste; compressive strength; sulfate attack; durability; deterioration mechanism

1. Introduction

The production of ordinary Portland cement (OPC) is highly energy-intensive and consumes substantial natural resources, while also generating high greenhouse gas (GHG) emissions. As a result, the cement industry becomes one of the major contributors to the environment and climate. Therefore, it is necessary to explore low-carbon, energy-saving and environment-friendly cementitious materials to partially replace OPC [1–3]. Fly ash-based geopolymer (FABG) is a new green low-carbon cementitious material produced through the alkali activation of fly ash, an industrial by-product rich in silicon and aluminum [4]. Compared with OPC production, geopolymer production can reduce CO_2 emission by approximately 50–80% [5]. Salas et al. [6] conducted a life cycle assessment of geopolymer concrete and reported that its global warming potential (GWP) is only about 64%

compared to OPC-based concrete. Therefore, the use of FABG not only reduces the environmental impact associated with cement production but also promotes the beneficial utilization of fly ash waste generated by coal-fired power plants, contributing to resource conservation and sustainable development.

Sulfate attack is one of the most critical durability issues affecting cementitious materials exposed to aggressive environments. In OPC systems, sulfate ions react with calcium-rich hydration products to form expansive phases such as gypsum and ettringite. The formation and growth of these products generate crystallization and expansion stresses within the matrix, which can eventually exceed the tensile strength of the material and result in cracking, spalling, and structural deterioration [7]. In contrast, the hydration products of geopolymer are mainly N-A-S-H gels. Consequently, the mechanisms governing sulfate-induced degradation in geopolymers differ fundamentally from those in OPC-based material.

Numerous studies have demonstrated that FABGs exhibit relatively high resistance to Na_2SO_4 attack [8–11]. Owing to the absence or limited content of calcium-rich hydration products, the formation of expansive phases such as gypsum and ettringite is largely suppressed, thereby reducing the risk of severe expansion and cracking [8]. In some cases, exposure to Na_2SO_4 solution even leads to a slight increase in compressive strength, which is attributed to continued geopolymerization and pore refinement during immersion [9]. Compared to Na_2SO_4, $MgSO_4$ is widely recognized as significantly more aggressive toward cement-based materials. This is primarily due to the dual role of Mg^{2+} and SO_4^{2-} ions in inducing chemical and structural degradation [12–14].

Different studies employ varying sulfate concentrations, exposure durations, and testing methods, leading to inconsistent conclusions. A systematic comparison between Na_2SO_4 and $MgSO_4$ under controlled conditions is still lacking, particularly for geopolymer-based materials [15]. Therefore, it is necessary to conduct a systematic investigation on the degradation mechanism of geopolymer-based materials in different sulfate environments, so as to provide theoretical basis for the durability design specification of geopolymer-based concrete structure subjected to sulfate erosion in the future.

Based on the above background, geopolymer paste (GP) was prepared and subjected to Na_2SO_4 and $MgSO_4$ solutions. These two sulfate salts are the most prevalent aggressive species in marine environments, coastal soils, and industrial waste disposal sites, where geopolymer materials are increasingly being deployed as sustainable alternatives to Portland cement concrete. A systematic comparison of their degradation mechanisms is therefore critical for guiding material selection and durability design in sulfate-rich engineering applications. The performance of GP subjected to Na_2SO_4 and $MgSO_4$ solutions was investigated and compared in terms of appearance investigation, compressive strength, and microstructure.

2. Materials and Methods

2.1. Materials

Fly ash from Tianjin Dagang Power Plant of North China Electric Power Group Corporation was purchased from Tianjin Zhucheng New Material Technology Co., Tianjin, China. The chemical composition of fly ash was measured by X-ray fluorescence spectrometer and the results are presented in Table 1.

The micro-morphology of fly ash (Figure 1) was measured by a field emission scanning electron microscope (JSM-7500F, JEOL, Tokyo, Japan). The size grading curve of fly ash (Figure 2) was measured by the laser particle size analyzer (JL-6000, Chengdu Jingxin Power Testing Equipment Co., Chengdu, China).

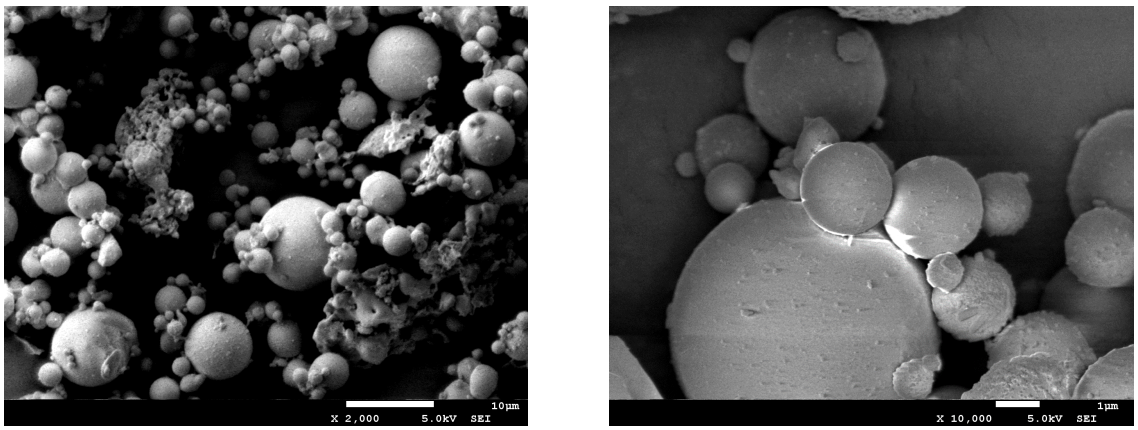

(**a**) (**b**)

Figure 1. Microscopic morphology of fly ash at magnification powers of 2000× (**a**) and 10,000× (**b**).

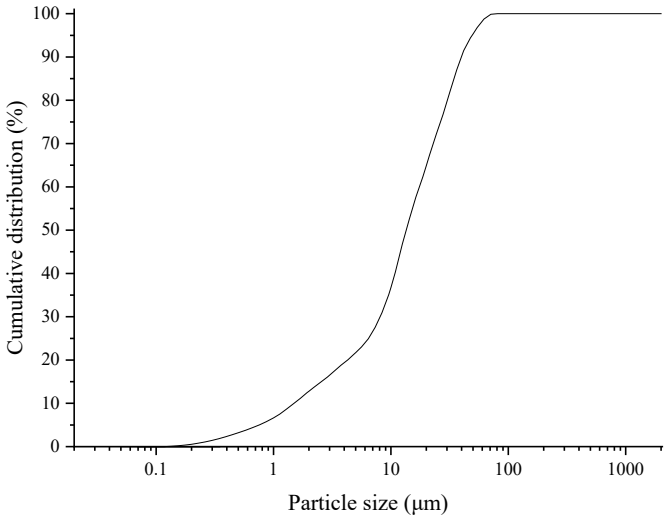

Figure 2. Gradation curve of fly ash.

Table 1. The main chemical composition of fly ash (as weight percentage, %).

Components	SiO_2	Al_2O_3	CaO	Fe_2O_3	MgO	K_2O	SO_3	P_2O_5	TiO_2	Na_2O	LOI *
Fly ash	60.8	15.89	6.92	9.27	0.80	0	0.11	3.22	1.14	0.97	0.88

* LOI means loss on ignition.

Sodium hydroxide (NaOH) solution, sodium sulfate solution and magnesium sulfate solution were prepared using analytically pure flake NaOH, analytically pure anhydrous sodium sulfate and anhydrous magnesium sulfate (Chengdu Kelong Chemical Reagent Factory, Chengdu, China). Sodium silicate (Na_2SiO_3) ZF32-40A was purchased from Foshan Zhongfa Waterglass Factory, Foshan, China, which is light yellow colloidal liquid (Table 2). The concentration of NaOH solution is 10 mol/L and the modulus of Na_2SiO_3 is 3.23 (Na_2O = 8.83%, SiO_2 = 27.64%, and H_2O = 63.53% by mass). The activator is composed of NaOH solution and Na_2SiO_3 solution, with a Na_2SiO_3 to NaOH mass ratio of 2.5. The activator to fly ash ratio is 0.35. The detailed mixture for geopolymer paste is shown in Table 3.

Table 2. Parameters of sodium silicate.

Appearance	SiO_2 Content	Na_2O Content	Modulus *	Density (20 °C)	Water Insoluble Matter	Fe Content
High definition transparent viscous liquid	27.64%	8.83%	3.23	1.384 g/cm^3	0.01%	0.01%

* is the value of SiO_2/Na_2O ratio.

Table 3. The mix ratio of geopolymer paste (kg/m^3).

Fly Ash	NaOH	Na_2SiO_3	Activator/Fly Ash Ratio
623	62	156	0.35

2.2. Geopolymer Paste Preparation

The geopolymer pastes were cast into steel molds with dimensions of 40 mm × 40 mm × 160 mm. A total of 39 samples were prepared and divided into two groups according to the different cation types of the corrosion solution (Na_2SO_4 and $MgSO_4$), with 18 specimens per group and 3 additional non-corroded specimens serving as control. Among the 18 specimens, 9 specimens were used for appearance observation during sulfate exposure, while the remaining 9 specimens were used for compressive strength testing at the designated exposure ages. Additionally, two cubic specimens with dimension of 40 mm were also prepared for X-CT test. In order to fully integrate NaOH solution and sodium silicate, alkali activation solution was prepared 24 h in advance. Fly ash was weighed to reach the targeted mix ratio design, then a cement paste mixer was used to mix fly ash and alkali activation solution. After mixing for 1 min, the freshly mixed geopolymer paste was poured into the cement mortar steel test mold and vibrated for 30 s. The geopolymer paste was cured in an oven at 80 °C for 24 h. After demolding and labeling, the specimens were placed under ambient conditions at approximately 20 °C and 65% relative humidity for further curing. The detailed GP preparation procedure is shown in Figure 3.

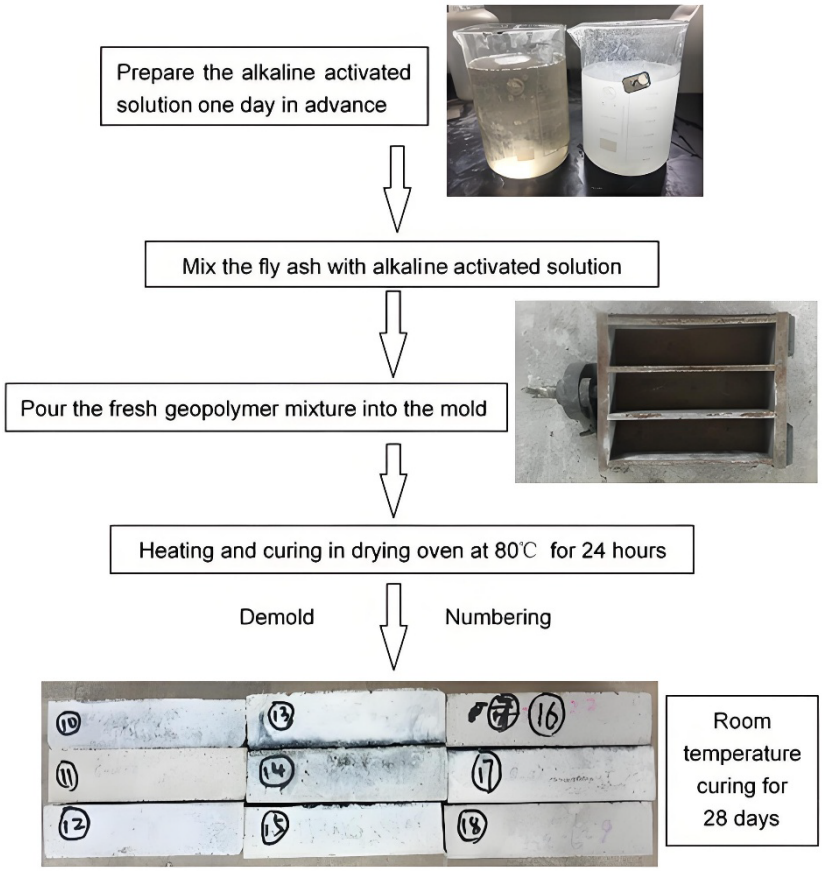

Figure 3. Flow chart for preparing specimens.

2.3. Analytical Methods

After 28 days of curing at room temperature, the specimens No. 1–18 were immersed in 8% Na_2SO_4 solution, and the specimens No. 19–36 were immersed in 8% $MgSO_4$ solution for 120 days. At 30-day intervals of immersion in the sulfate solution, surface changes of the specimens were observed, and their mass and compressive strength were tested.

During the sulfate exposure tests, the specimens were fully immersed in Na_2SO_4 or $MgSO_4$ solution, with the solution level maintained at least 10 mm above the top surface of the specimens. The sulfate solutions were not renewed throughout the 120-day exposure period, as the immersion solutions were collected for subsequent ICP-OES and pH analyses after the exposure. All immersion tests were conducted at room temperature of approximately 20 °C. Before each mass measurement, the specimen surfaces were gently wiped with a damp cloth to remove excess solution.

X-ray computed tomography (X-ray CT) test was performed by micro-CT imaging system (VivaCT 80, Scanco Medical AG, Bassersdorf, Switzerland). Two specimens measuring 40 mm × 40 mm × 40 mm were firstly subjected to X-ray CT test and then the specimens were subjected to Na_2SO_4 and $MgSO_4$ solutions, respectively. After 120 days of immersion, the two specimens were scanned with X-ray CT again to obtain the internal details of GP. During the X-ray CT test, the specimen was scanned from top to bottom at an interval of 0.05 mm over a total height of 20 mm, yielding 400 cross-sectional images for each specimen. The spatial resolution of the imaging system was 50 μm, allowing the detection of pores with diameters larger than 50 μm. X-ray computed tomography (CT) scanning was performed at a voltage of 70 kVp and a current of 114 μA, corresponding to an X-ray output power of 8 W. A 0.5 mm aluminum filter was applied during scanning, and beam hardening correction calibrated at 1200 mg HA/ccm was employed to minimize imaging artifacts. The reconstructed images had a voxel size of 30 μm and were generated using the built-in reconstruction software of the CT system for further visualization and analysis of internal pore structures.

In order to observe the microstructure and morphology of the GP before and after the sulfate solution erosion, SEM and EDS were carried out using Field Emission Scanning Electron Microscope (JSM-7500F, JEOL, Tokyo, Japan) equipped with EDS. XRD was conducted by X-ray diffractometer (EMPYREAN, PANalytical, Almelo, Netherlands). FTIR analysis was done by Fourier transform infrared spectrometer (Nicolet 6700, Thermo Scientific, Waltham, MA, USA). TGA was conducted by thermal analysis system (TGA/DSC2, METTLER

TOLEDO, Zurich, Switzerland). The thermal analysis experiments were used to determine the phase analysis of GP before and after sulfate attack. To detect the concentration changes of silicon and aluminum before and after immersion in the corrosion solution, inductively coupled plasma optical emission spectrometer (ICP-OES) was determined by the plasma emission spectrometer (5100SVDV, Agilent Technologies, Inc., Santa Clara, CA, USA). The pH values before and after immersion in the erosion solution were detected by pen-type acidity meter (pH-100A/100B, Bangxi Instrument Technology Co., Shanghai, China). The sulfate solutions were not renewed during the 120-day exposure period. After exposure, the immersion solutions were collected for ICP-OES and pH analyses.

It is essential to state that SEM/EDS, XRD, FTIR, and TGA/DTG analyses were conducted using representative fragments or powdered samples collected from the specimens after the compressive strength tests, whereas ICP-OES and pH measurements were performed using the immersion solutions collected at the designated exposure ages. Therefore, no additional prism specimens were required for these analyses.

3. Results and Discussion

3.1. Physical Properties

3.1.1. Appearance Changes

The surface changes of GP specimens before and after exposure to Na_2SO_4 solution are presented in Figure 4. Compared with the untreated GP (Figure 4a), powdered and granular Na_2SO_4 crystals were observed on the surface of GP after immersion in Na_2SO_4 solution (Figure 4d). After 30 days of corrosion with Na_2SO_4 solution, specimen No. 17 failed completely (Figure 4b) due to sulfate solution penetration to internal cracks. With prolonged immersion for 60 days, specimens No. 12 also broke (Figure 4c). Furthermore, after 120 days of soaking in Na_2SO_4 solution, spalling and fragmentation were observed in three GP specimens (Figure 4d).

(**a**) Before exposure

(**b**) After 30 days exposure

(**c**) After 60 days exposure

(**d**) After 120 days exposure

Figure 4. The appearance damage of the geopolymer paste before and after Na_2SO_4 exposure.

The surface changes of GP specimens before and after exposure to $MgSO_4$ solution are presented in Figure 5. Compared with the GP before exposure to $MgSO_4$ solution (Figure 5a), massive $MgSO_4$ crystals formed on the surface of GP after $MgSO_4$ solution erosion, with almost no spalling fragments observed. After 30 days of exposure to $MgSO_4$ solution, two specimens (No. 30 and No. 36) were broken into two segments due to through crack, and $MgSO_4$ crystals were concentrated along the cracks (Figure 5b). After being eroded by $MgSO_4$ solution for 60 days, the specimen No. 36 was broken into three sections due to the penetration of the solution to the two cracks. The specimen No. 33 also fractured at the place where $MgSO_4$ crystals were enriched (Figure 5c). After 120 days of $MgSO_4$ solution corrosion, the specimen No. 31 was also broken into two segments due to through cracks (Figure 5d).

(**a**) Before exposure

(**b**) After 30 days exposure

(**c**) After 60 days exposure

(**d**) After 120 days exposure

Figure 5. The appearance damage of the geopolymer paste before and after $MgSO_4$ exposure.

The erosion of GP by Na_2SO_4 solution and $MgSO_4$ solution showed different effects on appearance damage. Comparatively, Na_2SO_4 crystals appeared as powdered particles on the surface of GP, while $MgSO_4$ crystals were blocky on the surface of the GP. In each group of 9 samples, there are 2 through cracks in the specimens eroded by Na_2SO_4 solution, while 5 through cracks in the specimens eroded by $MgSO_4$ solution. The $MgSO_4$ solution erosion resulted in more through cracks in the GP specimens. In addition, it can be concluded that Na_2SO_4 solution erosion makes GP flake, while $MgSO_4$ solution erosion hardly makes GP flake. These appearance damage phenomena confirm that the erosion of $MgSO_4$ solution makes it easier to connect the pores in the GP, resulting in the formation of more through cracks. Moreover, the erosion mechanisms of Na_2SO_4 and $MgSO_4$ on GP are inconsistent, and the differences of erosion mechanism were analyzed in the subsequent microscopic analysis.

Rashidian-Dezfouli and Rangaraju [16] found that there were no visible cracks or spalling on the surface of geopolymer mortar after soaking in 5% Na_2SO_4 solution for 120 days. In addition, Bakharev [17] confirmed that soaking of GP in a 5% $MgSO_4$ solution for 150 days resulted in no sediment on the surface of the sample, and it was as smooth as before the untreated. However, the present results showed that the mass fraction of the sulfate attack solution in this experiment is 8%, which confirms that increasing of mass fraction of the sulfate solution (Na_2SO_4 or $MgSO_4$) from 5% to 8%, increased the damage degree of the GP.

3.1.2. Mass Changes

The mass changes of GP after exposure to 8% Na_2SO_4 and $MgSO_4$ solutions are shown in Figure 6. It can be seen that the mass increased significantly by 8.35% and 8.57%, respectively, after 30 days exposure to Na_2SO_4 and $MgSO_4$ solutions. Since the initial mass of GP before sulfate solution exposure is measured in the dry state and the specimens have a certain water absorption capacity, the observed mass gain during the early stage of exposure is primarily attributed to sulfate solution uptake. Comparatively, the mass growth rate of GP in $MgSO_4$ solution was slightly higher than that in Na_2SO_4 solution. It might be attributed to the higher precipitation of $MgSO_4$ crystals than Na_2SO_4 on the surface, as discussed in the previous section. With prolonged exposure, the mass evolution of GP differed in the two sulfate environments (Figure 6). The mass gain gradually decreased from 8.35% at 30 days to 7.76% at 120 days in Na_2SO_4 solution. In contrast, the mass gain in $MgSO_4$ decreased slightly after 60 days to about 8.35% and then remained almost stable up to 120 days. The lower mass growth rate of GP in the Na_2SO_4 solution is also related to the spalling of specimens during sulfate attack, which partially offset the mass increase caused by water absorption and reaction-product accumulation.

Bakharev [17] found that the mass of GP activated by sodium silicate and NaOH solutions increased by 1.4–5.3% after soaking in 5% Na_2SO_4 and $MgSO_4$ solution for 150 days. The liquid-solid ratio in that study was 0.3, and the liquid-solid ratio in this present experiment is 0.35. The increase of liquid-solid ratio increases the water absorption of GP [18], leading to higher mass change rate of GP. Therefore, the mass growth rate of the GP tested in the present experiment is higher than the quality growth rate studied by Bakharev [17].

3.2. Compressive Performance

The variation in compressive strength and compressive strength loss rate of GP after soaking in the two studied sulfate solutions up to 120 days are shown in Figure 7. The compressive strength of the GP specimen subjected to Na_2SO_4 solution exhibited a two-stage rapid decline with the increasing exposure time. The first significant reduction occurred between 30–60 days and the second stage was between 90 and 120 days. However, the compressive strength of GP exposed to $MgSO_4$ solution decreased gradually with the increasing immersion time. Overall, the compressive strength in Na_2SO_4 solution was lower than that of $MgSO_4$ at all studied erosion times. After 120 days of immersion, the compressive strength loss rates of GP were 40.2% and 34.0% in Na_2SO_4

and $MgSO_4$ solutions, respectively (Figure 7b), indicating that the degradation degree of GP in Na_2SO_4 solution is more serious than that in $MgSO_4$ solution, which is consistent with previous findings [18]. The subsequent microstructure analysis is important to elucidate the higher strength of the specimen after $MgSO_4$ erosion than that after Na_2SO_4 erosion (Section 3.3).

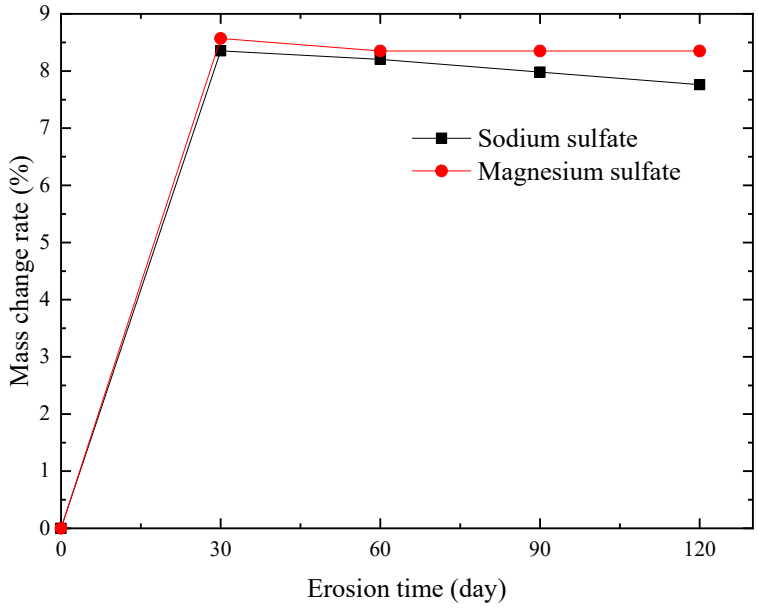

Figure 6. Mass change of GP after exposure to Na_2SO_4 and $MgSO_4$ solutions.

Duan et al. [19] used 5% Na_2SO_4 solution for the treatment of FABG paste for 180 days, and recorded 19.6% loss rate in its compressive strength. However, the present study used 8% Na_2SO_4 solution showed 40.2% compressive strength loss rate reached after 120 days of erosion. Thus, the increase of Na_2SO_4 concentration significantly accelerated the deterioration of GP. Elyamany et al. [20] found that the compressive strength loss rate of geopolymer mortar activated with 10 mol/L NaOH reached approximately 21% after 120 days of immersion in a 10% $MgSO_4$ solution. Although the mass fraction of $MgSO_4$ solution in the present study (8%) is lower, the GP specimens still exhibited a higher strength loss. This discrepancy may be attributed to the use of mortar specimens in the study by Elyamany et al. [20], where the incorporation of fine aggregates improved matrix compactness and enhanced resistance to sulfate attack.

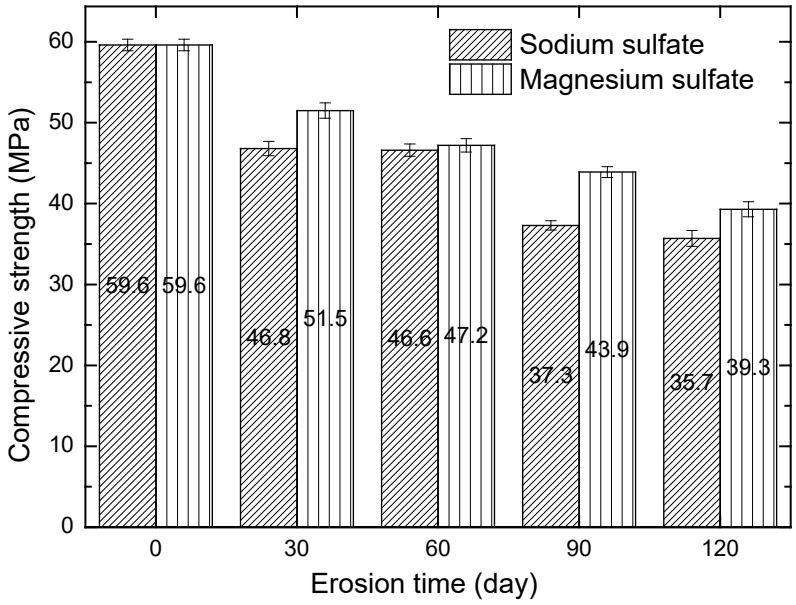

(**a**) Compressive strength variation of geopolymer paste after sulfate solution exposure

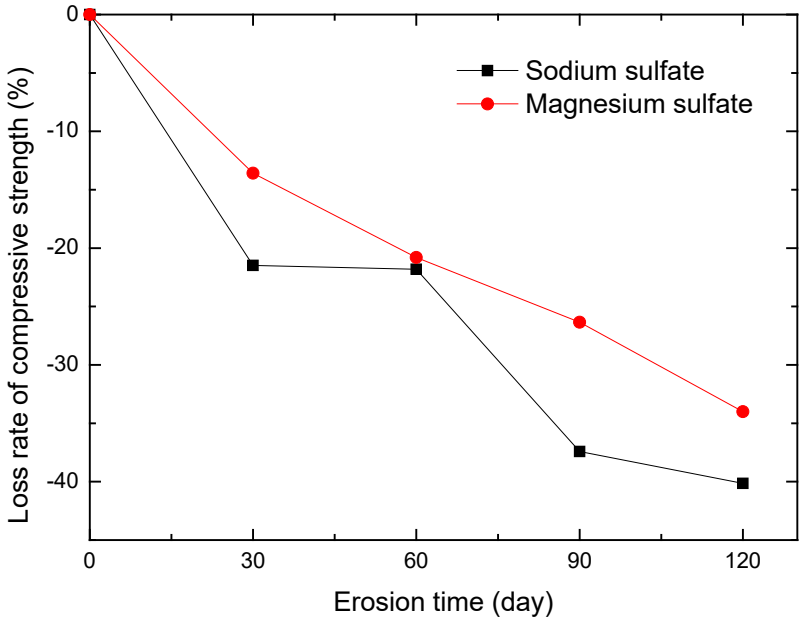

(**b**) Loss rate of compressive strength

Figure 7. Compressive strength variation and loss rate of GP after sulfate exposure.

Notably, the evolution of mechanical deterioration did not correspond directly to the degree of visible surface damage. Despite the formation of more extensive through-cracks under $MgSO_4$, Na_2SO_4 attack resulted in a greater reduction in compressive strength. Na_2SO_4 erosion primarily generates a widespread network of internal micro-cracks due to chemical expansion, which severely degrades the integral load-bearing capacity of GP. In contrast, $MgSO_4$ primarily caused localized macro-cracks and through-cracks, while the surrounding matrix remained relatively intact, resulting in a smaller reduction in compressive strength. Therefore, durability evaluation based solely on surface cracking or porosity may be insufficient.

3.3. Microstructure Examination

3.3.1. X-ray CT Analysis

The representative cross-sections of GP specimens before and after 120 days of sulfate solution attack are shown in Figure 8. After immersion, distinct differences in the internal deterioration patterns are observed. Specimens exposed to Na_2SO_4 solution exhibited noticeable internal exfoliation and material loss, whereas such damage was rarely observed in specimens immersed in $MgSO_4$ solution, which is inconsistent with the surface deterioration characteristics discussed in Section 3.1.1. In addition, no obvious internal cracks were detected in the GP specimens exposed to Na_2SO_4 solution, while distinct cracks developed in the specimens subjected to $MgSO_4$ attack. The appearance of cracks shows that $MgSO_4$ exposure caused more pronounced localized cracking damage. These results suggest Na_2SO_4 and $MgSO_4$ induce different deterioration mechanisms in GP. The underlying differences in the sulfate attack mechanism will be further analyzed in detail (Sections 3.3.2–3.3.6).

Chen et al. [21] recorded a large number of microcracks in cement mortar after six months of semi-immersion in 10% Na_2SO_4 solution. Qi et al. [22] conducted dry-wet cyclic erosion tests on recycled concrete containing 100% recycled aggregates using Na_2SO_4 solution with a concentration of 50 g/L. The results showed that microcracks not only appeared on the surface of the sample but also within the interface transition zone between cement paste and recycled aggregates. In contrast, no obvious microcracks were observed in the GP specimens exposed to Na_2SO_4 solution in the present study, which suggests that the deterioration mechanism of Na_2SO_4 attack on geopolymer materials differs from that on cement-based materials.

Based on the reconstruction of 400 CT scan images, the pore size and spatial distribution within the sample are visualized, as shown in Figure 9. Sulfate exposure in both Na_2SO_4 and $MgSO_4$ increased the pores of GP specimens, indicating an increase in the detectable internal voids. However, the evolution of pore size differed significantly between the two sulfate environments. The detectable maximum pore diameter decreased from 2.85 mm to 2.25 mm after Na_2SO_4 solution exposure, whereas it increased from 2.3 mm to 2.65 mm after $MgSO_4$ solution attack. The reduction in the maximum diameter under Na_2SO_4 exposure may be attributed to the spalling of loose fragments or the formation of reaction products that partially filled larger pores. However, this interpretation should be

regarded as a possible explanation rather than direct evidence from CT analysis. By contrast, the increase in the maximum diameter after $MgSO_4$ exposure is consistent with the development of larger detectable voids, which may be associated with crystallization and expansion processes within the pore network. $MgSO_4$ may crystallize within the pores and generate crystallization pressure, thereby contributing to the enlargement of detectable internal pores.

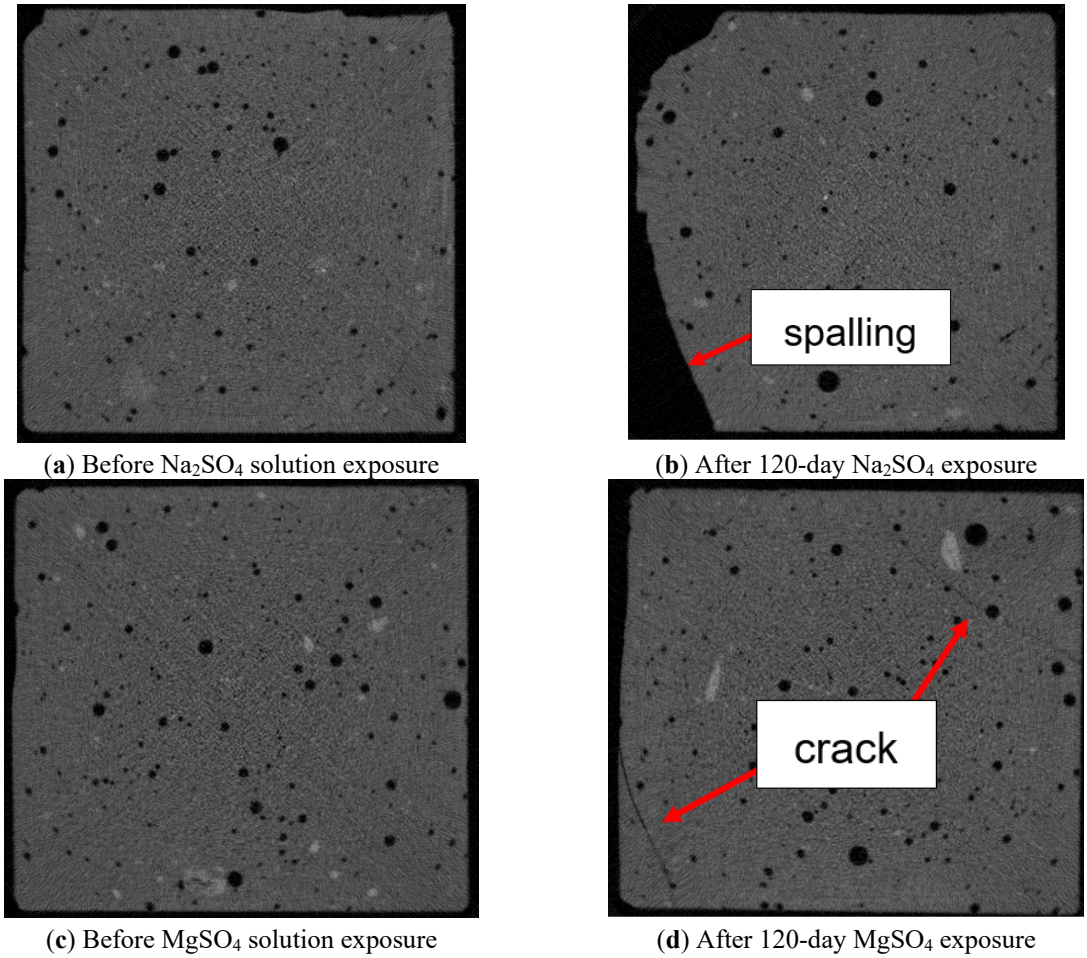

(**a**) Before Na_2SO_4 solution exposure (**b**) After 120-day Na_2SO_4 exposure

(**c**) Before $MgSO_4$ solution exposure (**d**) After 120-day $MgSO_4$ exposure

Figure 8. X-ray CT scan cross-section image of geopolymer paste before and after sulfate solution.

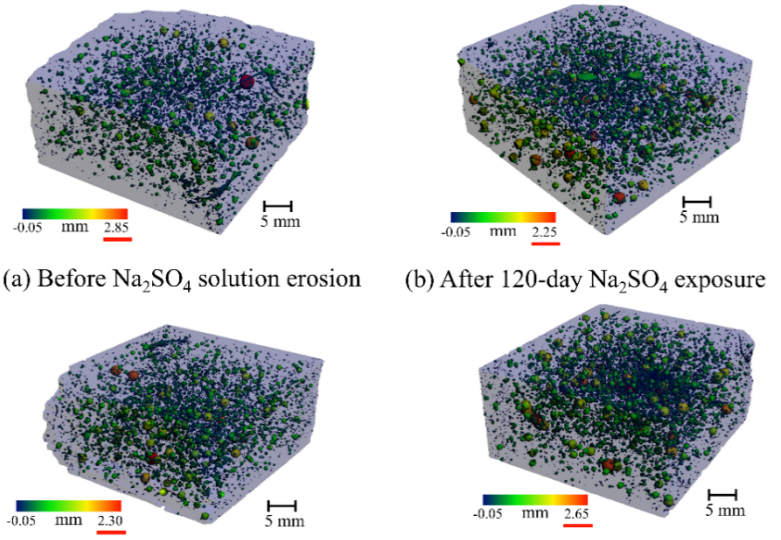

(a) Before Na_2SO_4 solution erosion (b) After 120-day Na_2SO_4 exposure

(c) Before $MgSO_4$ solution erosion (d) After 120-day $MgSO_4$ exposure

Figure 9. Three-dimensional reconstruction of pore size and distribution of geopolymer paste before and after sulfate attack for 120 days.

In addition, the void ratio before and after exposure to the sulfate attack were estimated using SCANCO software (vivaCT 80). The results and the change in void ratio are given in Table 4. As given in Table 4, the void ratio increased from 1.26 to 1.51 with an enhancement of 19.84% in Na_2SO_4 solution and the void ratio increased from 2.04 to 2.44 with an enhancement of 19.61% in $MgSO_4$ solution. Therefore, the GP specimens exhibited a greater increase in the CT-detectable void ratio after Na_2SO_4 exposure, which may be associated with its higher strength loss (Figure 7).

It should be noted that the CT observations in this study were based on paired scans of the representative specimens before and after sulfate exposure, and therefore provide supporting rather than statistically conclusive evidence of the internal deterioration mechanisms. Moreover, the CT resolution was 50 μm, meaning that microcracks and fine pores smaller than this scale could not be reliably detected. Therefore, the CT results should be interpreted together with the mechanical and microstructural characterization results.

Table 4. Void ratio variation of geopolymer paste before and after sulfate attack for 120 days.

	Initial Void Ratio	Void Ratio at 120 Days	Change in Void Ratio (%)
Na_2SO_4 solution	1.26	1.51	19.84
$MgSO_4$ solution	2.04	2.44	19.61

3.3.2. SEM and EDS Analysis

The micro-morphology and EDS results of GP samples before and after sulfate treatment are presented in Figure 10. In the untreated specimen, the morphology of the N-A-S-H gel exhibited a dense characteristic consisting of a blocky crystalline or an amorphous phase (Figure 10a). However, a newly formed amorphous gel phase was observed in the GP samples after exposure to Na_2SO_4 solution (Figure 10b). This newly observed phase may be associated with the deterioration and reorganization of the geopolymer matrix, which may contribute to the reduction in compressive strength.

The EDS results further revealed local changes in elemental composition. Compared with the untreated specimen, the sodium content of the GP exposed to Na_2SO_4 solution increased by a factor of 2.44 (Figure 10a,b). This enrichment of sodium suggested the accumulation and crystallization of Na_2SO_4 within GP sample. The possible presence of Na_2SO_4 crystals was further considered by combining the local EDS results with the morphological characteristics observed in the SEM images (Figure 10b). This observation provides supporting evidence for the X-ray CT results, which showed an increase in the detectable internal void ratio after Na_2SO_4 exposure.

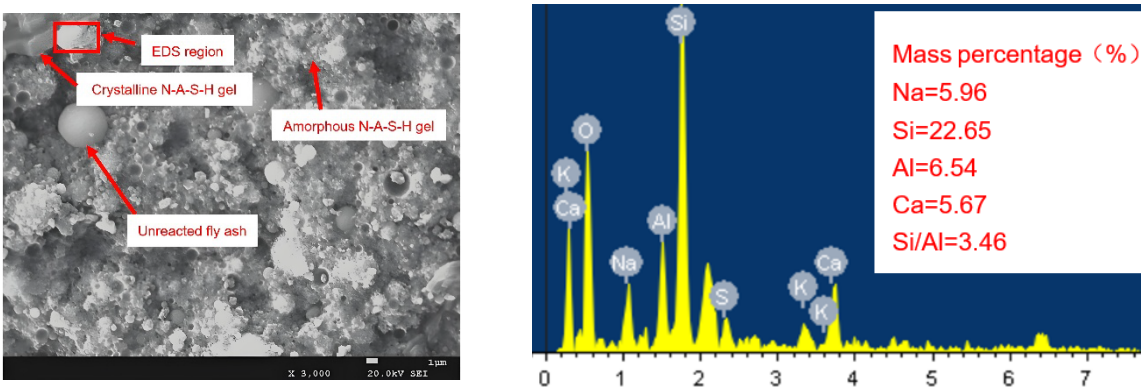

(**a**) SEM and EDS results of geopolymer paste without sulfate attack

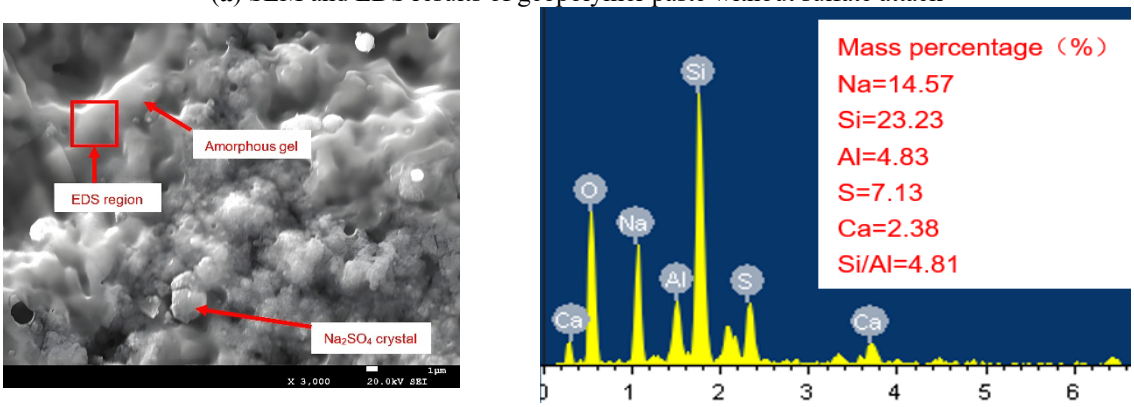

(**b**) SEM and EDS results of geopolymer paste after 120 days of sodium sulfate solution exposure

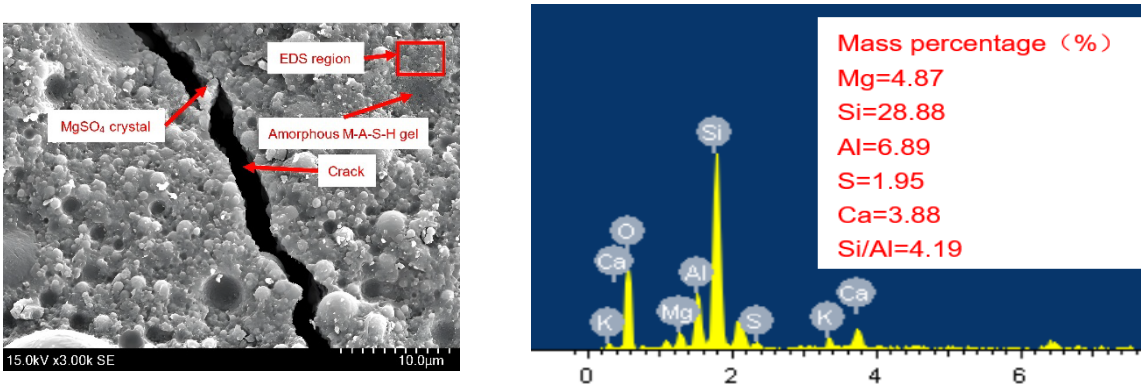

(**c**) SEM and EDS results of geopolymer paste after 120 days of $MgSO_4$ solution exposure

Figure 10. SEM and EDS results of geopolymer paste specimens before and after sulfate attack and the part in the red box is the area selected for energy spectrum analysis.

According to Figure 10c, Mg element was detected in the EDS spectrum of the GP samples exposed to $MgSO_4$ solution, while Na was not detected. This local Mg enrichment suggests that Mg^{2+} might have interacted with N-A-S-H gel. The observed Mg-containing amorphous phase may be consistent with the possible formation of M-A-S-H-type products; however, its formation cannot be conclusively confirmed based on the present SEM/EDS results alone (Figure 10c). In addition, a crack with a width of about 20 μm can be observed in the $MgSO_4$-attack specimen, whereas no cracks were identified in the specimen exposed to Na_2SO_4 solution. This observation is consistent with the X-ray CT results. Therefore, the observed cracking may be related to crystallization and expansion processes associated with $MgSO_4$ within the pore structure, which could contribute to the increase in internal porosity.

The relationship between Si/Al ratio and compressive strength has been reported in previous studies, as presented in Figure 11. Lee et al. [23] reported that the compressive strength of GP varied with the Si/Al ratio, reaching the highest value at a ratio of 3.5, followed by 1.5, whereas a ratio of 4.0 resulted in a substantially lower strength. In the present study, the Si/Al ratios obtained from EDS analysis were 3.46, 4.19, and 4.81 for the untreated, Na_2SO_4-exposed and $MgSO_4$-exposed specimens, respectively. As shown in Figure 11, the present data exhibit a similar decreasing trend in compressive strength as the EDS-derived Si/Al ratio increases beyond approximately 3.5.

However, this apparent relationship should be interpreted with caution because the Si/Al ratios obtained from EDS represent local chemical compositions and may not fully reflect the bulk composition of the geopolymer matrix. Therefore, the observed correlation does not necessarily indicate a direct causal relationship between the Si/Al ratio and compressive strength. Instead, the changes in the local Si/Al ratio may reflect sulfate-induced modifications of the aluminosilicate gel and associated microstructural changes.

3.3.3. XRD Analysis

The XRD results of GP samples before and after sulfate solution exposure are shown in Figure 12. The diffraction peaks were identified and analyzed using MDI Jade 6.5 by comparing the characteristic diffraction angles of the major crystalline phases. As shown in Figure 12, quartz (SiO_2), with characteristic peaks at approximately 20.8°, 26.6°, and 50.1° (2θ), and albite ($Na_2AlSi_3O_8$), with a characteristic peak around 27.9° (2θ), were identified in all three groups. These crystalline phases remained detectable after sulfate exposure, although their peak intensities changed to some extent. It should be noted that albite and other crystalline phases identified by distinct diffraction peaks should be distinguished from the N-A-S-H gel, which is the main binding phase of the geopolymer and is predominantly amorphous or poorly crystalline. Therefore, N-A-S-H is mainly reflected by the broad diffuse halo rather than distinct diffraction peaks. Weak changes in additional crystalline reflections after sulfate exposure may indicate alterations in the crystalline phase assemblage; however, the XRD results alone cannot confirm a direct transformation of N-A-S-H gel into a specific crystalline phase.

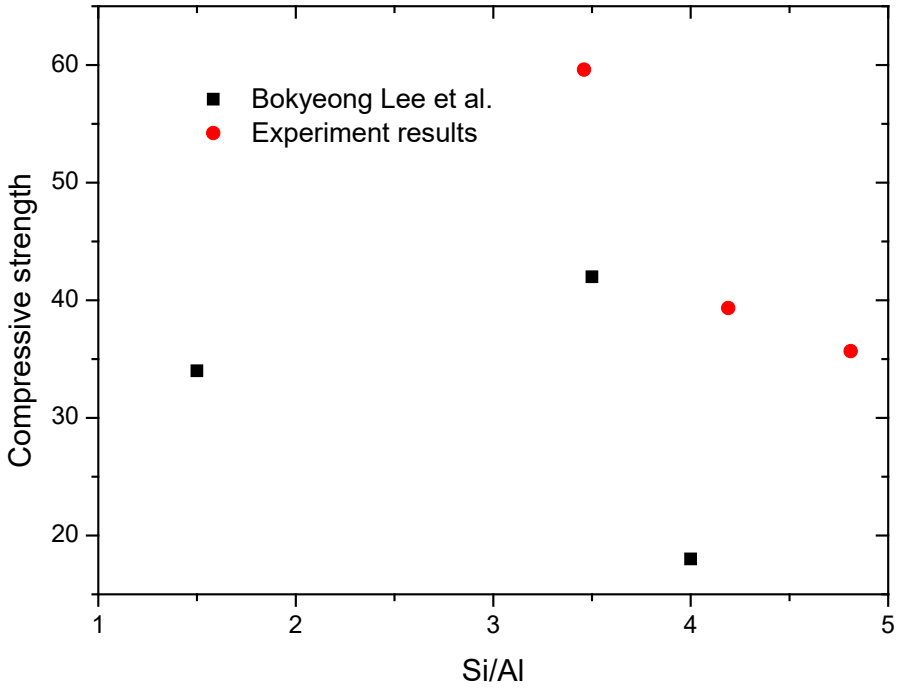

Figure 11. Relationship between compressive strength and Si/Al ratio: data from this study and Lee et al. [23].

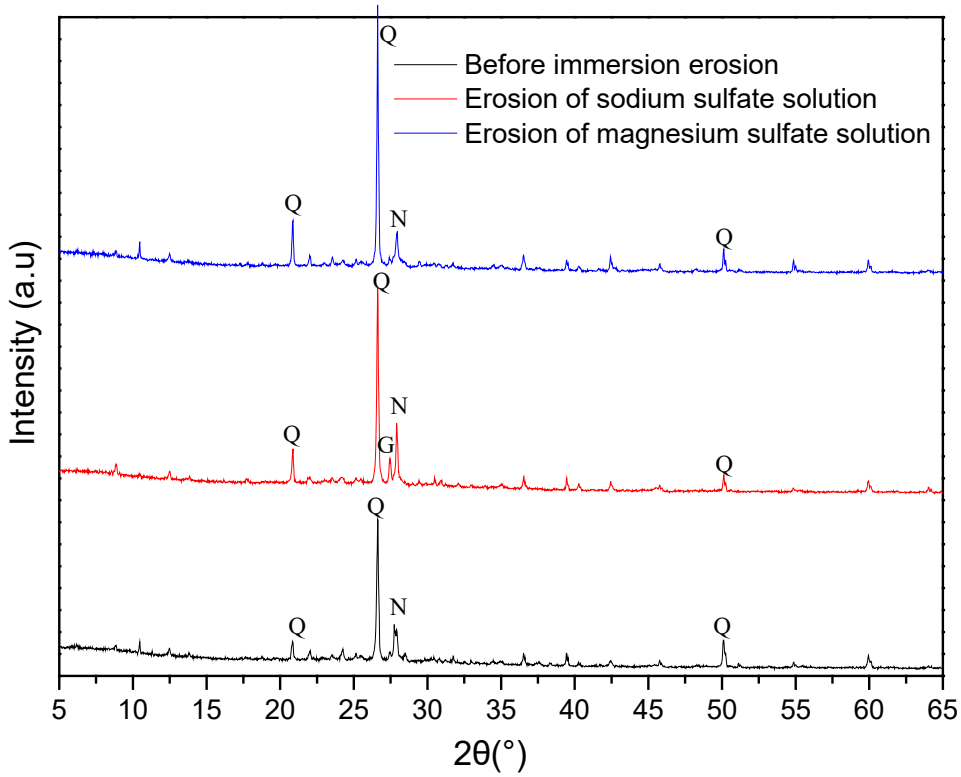

Figure 12. X-ray diffraction patterns of geopolymer before and after sulfate attack, Q: SiO_2, N: $Na_2AlSi_3O_8$, G: $NaAlSi_2O_6{\cdot}H_2O$.

Kwasny et al. [24] also identified the above two phases in the lithomarge-based geopolymer mortars. In the present study, albite remained detectable after sulfate exposure, and the diffraction peaks associated with this phase retained a high degree of crystallinity, indicating that albite exhibits relatively good stability in sulfate solution. However, in the GP samples exposed to Na_2SO_4 solution, an additional diffraction feature corresponding to $NaAlSi_2O_6{\cdot}H_2O$ (analcime) was identified at approximately 27.5° 2θ. The diffraction pattern analysis suggested a less ordered structure compared with that of albite. This observation indicates that Na_2SO_4 attack may alter the original aluminosilicate network, promoting the transformation of albite with a stable three-dimensional network

structure into an unstable two-dimensional plane structure analcime. Combined with the SEM observations, the newly formed amorphous or poorly crystalline gel phase observed after Na_2SO_4 exposure is likely associated with the formation of analcime or analcime-like reaction products.

3.3.4. FTIR Analysis

The FTIR spectra of GP specimens before and after sulfate exposure are shown in Figure 13. It should be noted upfront that vibrational bands from unreacted fly ash, aluminosilicate gels, sulfate salts, carbonate phases, and crystalline aluminosilicates frequently overlap in multi-phase geopolymer systems. For this reason, all peak assignments below are interpreted on a tentative, indicative basis rather than as definitive phase identification.

According to Nanru and Wenhai [25], the absorption peak near 784 cm^{-1} is typically ascribed to albite. This band was observed in all three samples, which is consistent with the XRD analysis results and supports that albite represents a major crystalline constituent associated with the N-A-S-H gel. In the untreated sample, an absorption peak near 615 cm^{-1} can be observed. This peak is usually linked to natrolite ($Na_2Al_2Si_3O_{10}\cdot 2H_2O$), and it suggests that natrolite probably existed in the original N-A-S-H gel matrix. As given in Figure 13b, a weak absorption peak appears near 600 cm^{-1} in Na_2SO_4-treated sample, which is related to the typical vibrational band of analcime. This observation is consistent with the XRD results and provides more supporting evidence that analcime may form during Na_2SO_4 attack. However, no distinct absorption peaks are observed near 615 cm^{-1} and 600 cm^{-1} in $MgSO_4$-treated sample. This result may suggest that natrolite is not stable under $MgSO_4$ attack, and it may change into other aluminosilicate phases. At the same time, we should also note that overlapping bands may cover the original peaks. This is also a possible reason for the observation.

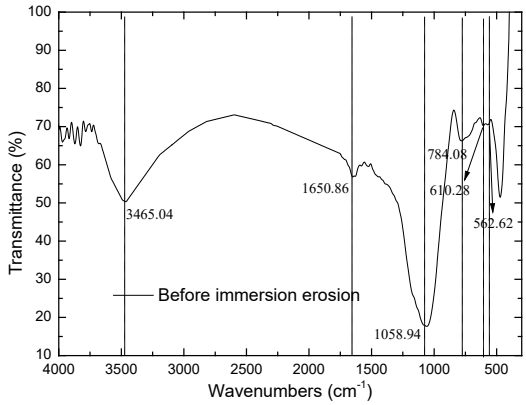

(**a**) Before immersion erosion

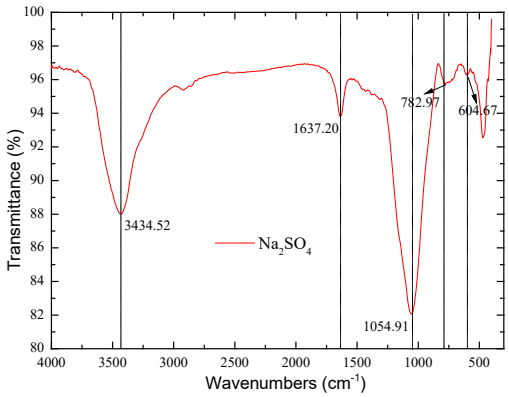

(**b**) After Na_2SO_4 exposure

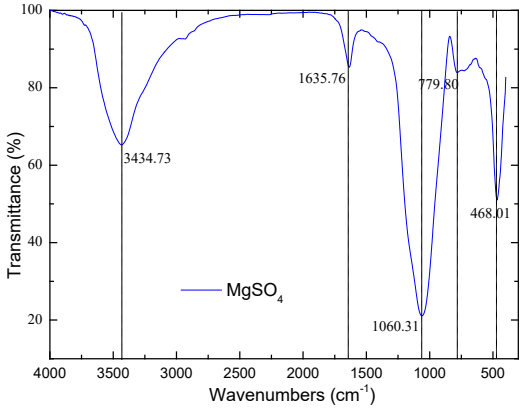

(**c**) After $MgSO_4$ exposure

Figure 13. FTIR spectra of geopolymer paste before and after sulfate attack for 120 days.

3.3.5. TG/DTG Analysis

The TG results of GP specimens before and after sulfate attack are shown in Figure 14. The untreated GP exhibited a total mass loss of 5.92%, whereas the GP samples exposed to Na_2SO_4 and $MgSO_4$ solutions showed slightly higher mass losses of 6.01% and 7.14%, respectively. The greater mass loss observed in the $MgSO_4$-treated specimen suggests more extensive alterations in the gel structure during sulfate attack. The DTG curves

provide further insight into the phase evolution of the GP samples. For the unexposed GP and the specimen exposed to Na_2SO_4 solution, the main mass loss peak was located at approximately 43 °C, indicating that there was a substance decomposition at this low temperature. However, the weight loss peak of GP exposed to $MgSO_4$ solution shifted to around 70 °C. According to Elyamany et al. [20], the dehydration peak at approximately 43 °C is generally attributed to N-A-S-H gels, while the peak around 70 °C may be related to Mg-containing gel phases, including M-A-S-H gels. This shift in dehydration temperature provides reasonable evidence that Mg^{2+} ions interacted with the original N-A-S-H gel, resulting in the formation of M-A-S-H gel. Therefore, the deterioration of GP in $MgSO_4$ solution can be attributed not only to salt crystallization and expansion-induced cracking, but also to the chemical transformation of the binding gel phase according to the following reaction:

$$\text{N-A-S-H} + Mg^{2+} \rightarrow \text{M-A-S-H} + Na^{+} \quad (1)$$

The formation of M-A-S-H gel alters the original aluminosilicate network structure and contributes to the progressive degradation of compressive strength during $MgSO_4$ exposure (Figure 7a). This finding is consistent with the SEM and EDS analysis discussed in Section 3.3.2.

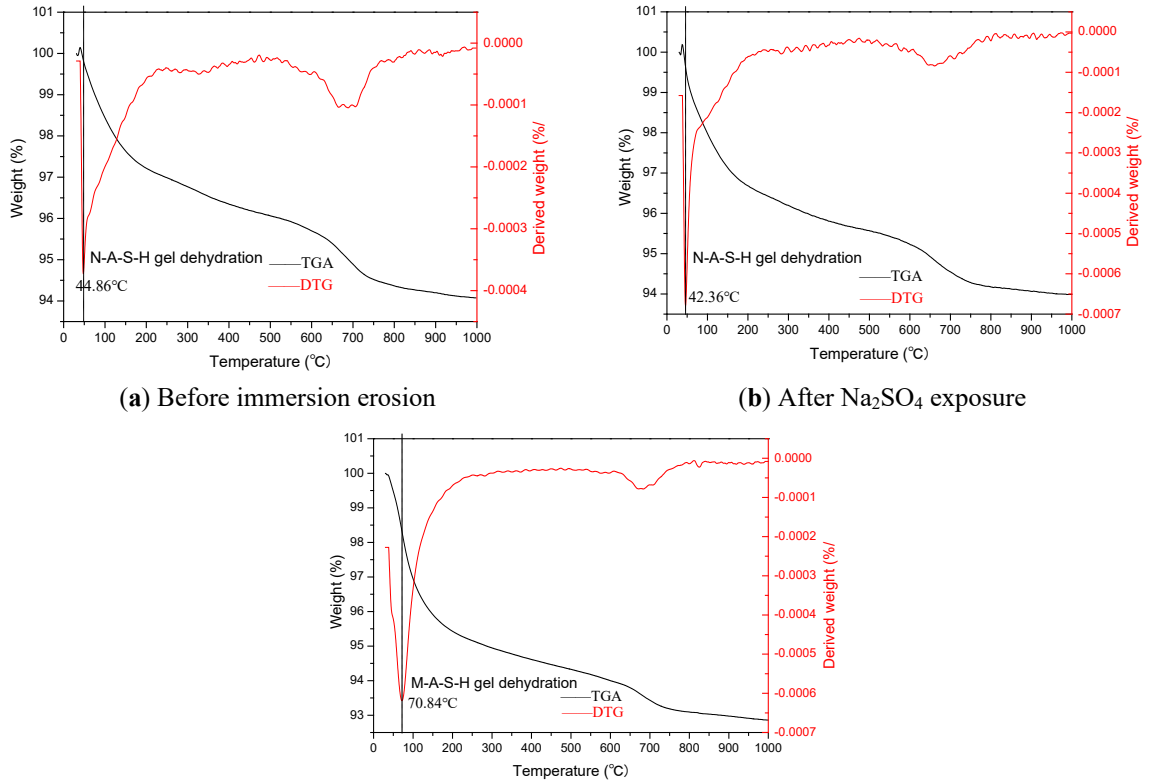

(**a**) Before immersion erosion (**b**) After Na_2SO_4 exposure

(**c**) After $MgSO_4$ exposure

Figure 14. TGA and DTG results of geopolymer paste before and after sulfate attack.

In addition, a secondary weight-loss peak was observed at approximately 650 °C, which can be attributed to the decomposition of carbonate minerals [26]. These carbonates were likely formed through the carbonation of residual calcium-containing phases. The presence of these carbonate phases indicates that limited carbonation occurred in the GP, although their contribution to the overall sulfate deterioration process appears to be relatively minor.

3.3.6. Sulfate Attack Solution Analysis

The Si and Al concentrations of Na_2SO_4 solution and $MgSO_4$ solution before and after attack obtained from ICP-OES tests are presented in Table 5. Additionally, the pH values of the sulfate attack solution are also shown in Table 5.

It can be seen from Table 5 that after 120 days of immersion in sulfate solution, the content of Si in GP increases 21 times in Na_2SO_4 solution and only 2.6 times in $MgSO_4$ solution. The content of Al in Na_2SO_4 and $MgSO_4$ solutions is quite small and almost unchanged. This indicates that the N-A-S-H gel in the GP samples release a lot of Si elements in Na_2SO_4 solution, only a small amount of Si elements are released in $MgSO_4$ solution, and negligible Al element is released in sulfate solution.

Table 5. Results of ICP-OES and pH.

Solution Type	Si Concentration (ug/mL)	Al Concentration (ug/mL)	pH
0-day Na_2SO_4	5.2	<0.2	7.01
120-day Na_2SO_4	109	<0.2	9.74
0-day $MgSO_4$	5.0	<0.2	6.94
120-day $MgSO_4$	13	<0.2	8.48

After sulfate attack, the increase in Si concentration in both Na_2SO_4 and $MgSO_4$ solutions is mainly associated with the dissolution and depolymerization of N-A-S-H gel. Under the erosion effect of sulfate attack, N-A-S-H gels gradually lose structural stability, leading to the release of soluble Si species into the external solution [27,28]. It is reported that the N-A-S-H gel would transform into M-A-S-H [29,30] by the counter-diffusion between Mg^{2+} and Na^{+}. Therefore, the soluble Si concentration in $MgSO_4$ solution is lower than that in Na_2SO_4 solution.

The pH value of both Na_2SO_4 and $MgSO_4$ solutions increased after 120 days of immersion, and the pH value of Na_2SO_4 solution was 9.74 which is higher than that of $MgSO_4$ solution with 8.48. It was reported that after 365 days of soaking in the Na_2SO_4 solution with 50 g/L concentration, the Na_2SO_4 solution would destroy the -Si-O-Si- bond in the N-A-S-H gel and release the element of the Si, resulting in an increase in the pH value of the solution in the solution [31]. Additionally, the leaching of OH^{-} and SiO_3^{2-} into sulfate solution would also be responsible for the increase of pH. However, in $MgSO_4$ solution, Mg^{2+} reacted with OH^{-} to precipitate brucite. This reaction continuously consumed OH^{-}, thereby reducing the alkalinity of the solution, which might be account for lower pH.

3.3.7. The Erosion Mechanism of Different Sulfate Solutions on GP

The existing studies demonstrated that the sulfate deterioration of alkali-activated slag systems is widely attributed primarily to the decalcification of C-(A)-S-H gel and the formation of expansive reaction products such as gypsum and ettringite under sulfate attack [32]. In contrast, the GP is predominantly composed of N-A-S-H gel [33], and might exhibits a different deterioration mechanism.

The combined results of compressive strength, XRD, FTIR, SEM and EDS suggest that sulfate attack mainly damages the structural stability of aluminosilicate network. After exposure to Na_2SO_4 solution, the weakening of characteristic albite diffraction peaks, together with the appearance of analcime phases, suggests changes in the mineral structure within the geopolymer matrix. These chemical and mineral changes are accompanied by increased porosity and surface damage found through CT and SEM imaging, which agrees with the measured gradual decrease in compressive strength. In addition, the crystallization of sodium sulfate salts within the pore structure may further worsen microcrack growth and pore expansion after long-term exposure.

Unlike the specimens exposed to Na_2SO_4 solution, the $MgSO_4$-exposed specimens followed a distinct deterioration process. EDS analysis suggests that magnesium may have entered the reaction products, while XRD detected no clear evidence of significant amounts of new crystalline magnesium-containing phases. Taken together with the DTG results, these findings support the possibility that magnesium-containing amorphous products may have formed. This is in line with previous studies that have reported M-A-S-H-type gels under $MgSO_4$ attack [34]. However, the existence and exact chemical composition of such gel phases cannot be fully verified based only on the currently available data. The inward diffusion of Mg^{2+} ions, along with sulfate salt crystallization and worsening microstructural damage, may gradually reduce the structural integrity of the geopolymer matrix, which likely causes the observed drop in compressive strength.

In summary, although both sulfate solutions resulted in strength degradation, Na_2SO_4 exposure primarily drove aluminosilicate framework destabilization coupled with expansive stress related to sodium sulfate crystallization. By contrast, $MgSO_4$ introduced additional Mg-related chemical interactions that altered the reaction products and induced progressive microstructural deterioration.

4. Conclusions

The effects of Na_2SO_4 and $MgSO_4$ solutions on the deterioration behavior of fly ash-based geopolymer (GP) up to 120 days were investigated through mechanical testing and multi-scale microstructural characterization. Based on the experimental results, the following conclusions can be drawn:

(1) Exposure to Na_2SO_4 and $MgSO_4$ solutions resulted in distinct deterioration patterns in GP specimens. As directly observed, Na_2SO_4 exposure mainly caused surface exfoliation, whereas $MgSO_4$ exposure induced more pronounced through-thickness cracking.

(2) After 120 days of immersion, the measured compressive strength loss rates reached 40.2% and 34.0% for specimens immersed in Na_2SO_4 and $MgSO_4$ solutions, respectively. These quantitative results suggest that Na_2SO_4 exposure led to more severe strength degradation under the tested conditions.

(3) For Na_2SO_4 attack, the characterization data may suggest partial disruption of the N-A-S-H gel structure and the possible formation of analcime-bearing phases. When combined with pore-scale sodium sulfate crystallization, these processes are associated with increased internal damage, which may account for the observed strength reduction and surface spalling.

(4) For $MgSO_4$ attack, the experimental evidence possibly indicates the partial transformation of N-A-S-H gel toward M-A-S-H-type amorphous phases, alongside sulfate crystallization that may drive pore expansion and crack propagation. Overall, these findings suggest that Na_2SO_4 and $MgSO_4$ degrade GP through notably different chemical and physical degradation pathways.

This study provides a comparative understanding of the deterioration behavior of GP under Na_2SO_4 and $MgSO_4$ exposure based on multi-scale characterization. Nevertheless, the present investigation was conducted using a single mix design and sulfate concentration. Future studies should further evaluate the durability performance of GP with different strength grades under various sulfate environments to establish a more comprehensive understanding of its long-term behavior. In addition, advanced characterization techniques, such as solid-state NMR, are expected to provide further insights into the structural evolution of aluminosilicate gels and the possible transformation between N-A-S-H and M-A-S-H gels. Moreover, quantitative analysis of sulfate transport and deterioration evolution, including sulfate concentration profiles, penetration depth, and deteriorated layer thickness, should be incorporated in future work through techniques such as elemental mapping and depth-dependent chemical characterization to further validate the proposed deterioration mechanisms.

Author Contributions

X.S.: Writing—reviewing and editing, supervision, resources, methodology, conceptualization. T.L.: Writing—original draft preparation, writing—reviewing and editing, investigation, data curation, visualization. H.Z.: Writing—reviewing and editing, funding acquisition, conceptualization. Q.W.: Writing—reviewing and editing, writing—original draft, investigation, validation. All authors have read and agreed to the published version of the manuscript.

Funding

We would like to thank the financial support from the Sichuan Provincial Engineering Research Center of City Solid Waste Energy and Building Materials Conversion and Utilization Technology (GF2024ZD02).

Data Availability Statement

Data will be made available on reasonable request.

Conflicts of Interest

The authors declare no conflict of interest. Given the role as Editor-in-Chief, Prof. Qingyuan Wang had no involvement in the peer review of this paper and had no access to information regarding its peer-review process. Full responsibility for the editorial process of this paper was delegated to another editor of the journal.

Use of AI and AI-Assisted Technologies

During the preparation of this work, the authors used ChatGPT to polish the manuscript. After using this tool/service, the authors reviewed and edited the content as needed and take full responsibility for the content of the published article.

References

1. Shi, C.; Qu, B.; Provis, J.L. Recent progress in low-carbon binders. *Cem. Concr. Res.* **2019**, *122*, 227–250. https://doi.org/10.1016/j.cemconres.2019.05.009.
2. Elahi, M.; Hossain, M.M.; Karim, M.R.; et al. A review on alkali-activated binders: Materials composition and fresh properties of concrete. *Constr. Build. Mater.* **2020**, *260*, 119788.
3. Metwally, G.A.M.; Elemam, W.E.; Mahdy, M.; et al. A comprehensive review of metakaolin-based ultra-high-performance geopolymer concrete enhanced with waste material additives. *J. Build. Eng.* **2025**, *103*, 112019. https://doi.org/10.1016/j.jobe.2025.112019.

4. Zhang, H.; Jia, T.C.; Sarker, P.K.; et al. Effect of fibre addition on the static and dynamic compressive properties of ambient-cured geopolymer concrete. *J. Build. Eng.* **2022**, *58*, 104991. https://doi.org/10.1016/j.jobe.2022.104991.
5. Duxson, P.; Provis, J.L.; Lukey, G.C.; et al. The role of inorganic polymer technology in the development of 'green concrete'. *Cem. Concr. Res.* **2007**, *37*, 1590–1597.
6. Salas, D.A.; Ramirez, A.D.; Ulloa, N.; et al. Life cycle assessment of geopolymer concrete. *Constr. Build. Mater.* **2018**, *190*, 170–177. https://doi.org/10.1016/j.conbuildmat.2018.09.123.
7. Yang, Y.; Gao, P.; Zhan, B.; et al. Influence of limestone powder particle size on the sulfate resistance of cement-based materials under the coupling effect of time-varying temperature and sulfate attack. *J. Build. Eng.* **2024**, *98*, 111271. https://doi.org/10.1016/j.jobe.2024.111271.
8. Ahmed, H. Effect of sulfate attack on fly ash/slag geopolymer mortar. *SVU Int. J. Eng. Sci. Appl.* **2025**, *6*, 142–151.
9. Ismail, I.; Bernal, S.A.; Provis, J.L.; et al. Microstructural changes in alkali activated fly ash/slag geopolymers with sulfate exposure. *Mater. Struct.* **2013**, *46*, 361–373.
10. Zerzouri Lakhssassi, M.; Alehyen, S.; El Alouani, M.; et al. The effect of aggressive environments on the properties of a low calcium fly ash based geopolymer and the ordinary Portland cement pastes. *Mater. Today Proc.* **2019**, *13*, 1169–1177. https://doi.org/10.1016/j.matpr.2019.04.085.
11. Yang, L.; Ma, B.; Zhu, Z.; et al. Mechanical and microstructural properties of one-part geopolymer-solidified soil attacked by Na_2SO_4. *J. Clean. Prod.* **2024**, *453*, 142241. https://doi.org/10.1016/j.jclepro.2024.142241.
12. Al-Kerttani, O.M.G.; Hilal, N.; Hama, S.M.; et al. Durability and hardened characteristics of cement mortar incorporating waste plastic and Polypropylene exposed to $MgSO_4$ attack. *Results Eng.* **2024**, *24*, 103310. https://doi.org/10.1016/j.rineng.2024.103310.
13. Gunjal, S.M.; Turkane, S.D.; Patankar, S.V.; et al. Effect of magnesium sulphate and sulphuric acid attack on limestone calcined clay cement concrete. *Mater. Today Proc.* **2023**. https://doi.org/10.1016/j.matpr.2023.03.488.
14. Zhang, Z.; Yin, H.; Hao, S.; et al. Study on the advancement process of alkali loss and deterioration of concrete under $MgSO_4$ erosion. *J. Mater. Res. Technol.* **2025**, *36*, 2849–2862. https://doi.org/10.1016/j.jmrt.2025.04.029.
15. Abdullah, H.H.; Shahin, M.A. Geomechanical properties of clay stabilised with fly ash-based geopolymer subjected to long-term sulfate attack. *Int. J. Geosynth. Ground Eng.* **2023**, *9*, 75.
16. Rashidian-Dezfouli, H.; Rangaraju, P.R. A comparative study on the durability of geopolymers produced with ground glass fiber, fly ash, and glass-powder in sodium sulfate solution. *Constr. Build. Mater.* **2017**, *153*, 996–1009.
17. Bakharev, T. Durability of geopolymer materials in sodium and magnesium sulfate solutions. *Cem. Concr. Res.* **2005**, *35*, 1233–1246.
18. Zhang, J.; Shi, C.; Zhang, Z.H.; et al. Durability of alkali-activated materials in aggressive environments: A review on recent studies. *Constr. Build. Mater.* **2017**, *152*, 598–613.
19. Duan, P.; Yan, C.; Zhou, W. Influence of partial replacement of fly ash by metakaolin on mechanical properties and microstructure of fly ash geopolymer paste exposed to sulfate attack. *Ceram. Int.* **2016**, *42*, 3504–3517.
20. Elyamany, H.E.; Abd Elmoaty, A.E.M.; Elshaboury, A.M. Magnesium sulfate resistance of geopolymer mortar. *Constr. Build. Mater.* **2018**, *184*, 111–127. https://doi.org/10.1016/j.conbuildmat.2018.06.212.
21. Chen, F.; Gao, J.; Qi, B.; et al. Deterioration mechanism of plain and blended cement mortars partially exposed to sulfate attack. *Constr. Build. Mater.* **2017**, *154*, 849–856.
22. Qi, B.; Gao, J.; Chen, F.; et al. Evaluation of the damage process of recycled aggregate concrete under sulfate attack and wetting-drying cycles. *Constr. Build. Mater.* **2017**, *138*, 254–262.
23. Lee, B.; Kim, G.; Kim, R.; et al. Strength development properties of geopolymer paste and mortar with respect to amorphous Si/Al ratio of fly ash. *Constr. Build. Mater.* **2017**, *151*, 512–519.
24. Kwasny, J.; Aiken, T.A.; Soutsos, M.N.; et al. Sulfate and acid resistance of lithomarge-based geopolymer mortars. *Constr. Build. Mater.* **2018**, *166*, 537–553.
25. Yang, N.; Yue, W. *The Handbook of Inorganic Metalloid Materials Atlas*; Wuhan University of Technology Press: Wuhan, China, 2000.
26. Khan, M.Z.N.; Shaikh, F.U.A.; Hao, Y.F.; et al. Synthesis of high strength ambient cured geopolymer composite by using low calcium fly ash. *Constr. Build. Mater.* **2016**, *125*, 809–820.
27. Tang, Q.; Sun, M.; Lu, X.; et al. Understanding erosion resistance mechanisms of sodium aluminate silicate hydrate in erosion environments: A molecular dynamics study. *RSC Adv.* **2024**, *14*, 10397–10408.
28. Chen, Y.; de Lima, L.M.; Li, Z.; et al. Synthesis, solubility and thermodynamic properties of NASH gels with various target Si/Al ratios. *Cem. Concr. Res.* **2024**, *180*, 107484.
29. Beltrame, N.A.M.; Kudlanvec, V.L.; Souto, R.; et al. Sulfate attack on geopolymer: Effect of the proportion of binder and air-entraining additive. *Rev. IBRACON Estrut. Mater.* **2024**, *17*, e17114.
30. Narattha, C.; Wattanasiriwech, S.; Wattanasiriwech, D. Effect of magnesium sulfate on properties of low calcium fly ash based-geopolymer-treated hemp shiv bio-concrete. *Constr. Build. Mater.* **2023**, *392*, 131714.

31. Baščarević, Z.; Komljenović, M.; Miladinović, Z.; et al. Impact of sodium sulfate solution on mechanical properties and structure of fly ash based geopolymers. *Mater. Struct.* **2015**, *48*, 683–697.
32. Gong, K.; White, C.E. Nanoscale chemical degradation mechanisms of sulfate attack in alkali-activated slag. *J. Phys. Chem. C* **2018**, *122*, 5992–6004.
33. Zhang, H.; Jiang, F.; Wang, Q.; et al. Influence of cement on properties of fly-ash-based concrete. *ACI Mater. J.* **2017**, *114*, 745–753. https://doi.org/10.14359/51700793.
34. Long, T.; Wang, Q.; Guan, Z.; et al. Deterioration and microstructural evolution of the fly ash geopolymer concrete against $MgSO_4$ solution. *Adv. Mater. Sci. Eng.* **2017**, *2017*, 4247217.